International Journal of Environmental Sciences
ISSN: 2229-7359
Vol. 11 No. 24s, 2025
https://theaspd.com/index.php

Adsorptive Removal Of Methylene Blue And Crystal Violet Dyes From Wastewater Through A Fixed-Bed Column Of Copper Oxide Nanoparticles

Tomar Nitika [1], Sharma Vivek [2] and Tomar Sapna[3*]
[1, 2]Department of Chemistry, Banasthali Vidyapith, Newai-304022, Rajasthan, India
[3*]Department of Chemistry, Agra College, Agra - 282002, Uttar Pradesh, India

Abstract
An effective and affordable technique of cleaning colored effluents was required due to the many detrimental impacts that dye-contaminated sewage has on the environment, human health, and other living things. Examples of agricultural waste that are produced in large quantities that are easily accessible and cheaply priced include sawdust, sugar cane bagasse, wheat husk, and coconut shells. Due to their abundance of functional groups with binding capabilities dye molecules, these lignocellulosic waste are effective and durable absorbents for wastewater treatment. This study uses a fixed-bed column filled with copper nanoparticles to look into the elimination of crystal violet and methylene blue from wastewater. The process variables being examined consist of input dye concentrations ranging from 200 to 600 mg/L, flow rates from 5 to 20 mL/min, and bed depths from 2 to 9 cm. FTIR detected Cu-O stretching vibrations and stabilizing chemicals, whereas BET analysis revealed a 10–100 m²/g mesoporous surface. FESEM showed 10-100 nm spherical to quasi-spherical CuNPs. FTIR and FESEM confirmed dye binding. Fixed-bed column studies at pH 7-9, 4-6 cm bed depth, and moderate temperatures of 25-35 °C revealed good adsorption. Adsorption occurred spontaneously and endothermically in spite of pseudo-second-order kinetics.
Keywords: *Copper oxide nanoparticles; Crystal violet, fixed-bed column; adsorption; methylene blue;*

Innovative Description
Copper oxide nanoparticles in fixed-bed columns remove up to 90% of dyes through electrostatic adsorption and pore diffusion, influenced by pH, temperature, and surface area.

1. INTRODUCTION

The rapid growth of the textile industry has intensified the problem of dye-polluted wastewater, which poses severe risks to human health and aquatic life due to the non-biodegradable and toxic nature of dyes [1]. Various treatment approaches—such as activated sludge, enzymatic degradation, electrolysis, photodegradation, chemical oxidation, filtration, precipitation, coagulation, and adsorption—have been explored for contaminant removal [2-4]. Among different nanomaterials, copper oxide nanoparticles (CuO NPs) have gained considerable attention because of their low cost, abundance, and wide applications in catalysis, electronics, and sensing [5,6]. However, their synthesis is often difficult due to low redox potential and susceptibility to oxidation [7]. The principles of sustainable chemistry are therefore crucial, as they guide the development of greener, safer, and more efficient synthesis methods that minimize pollution and hazardous waste [8–10]. Still, most conventional synthesis routes

remain costly and rely on toxic reagents [11]. CuO NPs have proven highly effective in dye removal, including methylene blue (MB) and crystal violet (CV), functioning both as adsorbents and catalysts. Their high surface area and electron-conducting ability enable the generation of reactive species such as hydroxyl and sulfate radicals, which break down dyes into harmless molecules through advanced oxidation processes (AOPs) [12–14]. Extensive research has also been conducted on metal nanoparticles (Au, Ag, Fe) and metal oxides like TiO_2, ZnO, and SnO_2, valued for their photocatalytic activity and stability. Recent advances include metal-oxide nanocomposites that improve charge separation and reduce electron–hole recombination, further enhancing degradation efficiency [15]. The performance of nanomaterials in dye degradation depends on several factors: light source, catalyst dosage, pH, initial dye concentration, and intrinsic properties such as band gap, porosity, and surface hydroxyl groups [16]. Overall, nanomaterials present significant benefits for wastewater treatment. They degrade even persistent dyes, can be synthesized via green methods, and offer cost-effective, scalable solutions for industrial applications [17].

2. EXPERIMENTAL SECTION

2.1 Materials

The materials used were hydrochloric acid, analytical-grade sodium hydroxide, and copper sulfate pentahydrate. HI Media Laboratories Private Limited is where the dyes CV and MB were bought.

2.2 Synthesis of Copper oxide nanoparticles

The procedure for synthesizing Copper oxide nanoparticles is described in detail. A standard procedure involved dissolving $CuSO4{\cdot}5H_2O$ (5g) in 10 mL of deionized water, then adding A 10% solution in 50 milliliters. at room temperature, the synthesis was conducted. After that, the mixture was heated to 100 °C while being constantly swirled for an hour. This process continued until the mixture turned dark brown. The product was centrifuged, filtered. To ensure purity, the precipitates were thoroughly rinsed multiple times with a distilled water–ethanol solution.

A visible hue shift suggested the development of copper oxide nanoparticles. In Figure 1.1(a, b), a reddish-brown solution represents the copper precursor at a reaction point, whereas in Figure 1.1(c, d), a translucent light green solution represents the precursor solution before the reaction or the supernatant after centrifugation and purification. Finally, in an oven, the nanoparticles were dried at low temperature [18,19].

Fig. 1 (a)

Fig. 1 (b)

Fig. 1 (c)

Fig. 1 (d)

Figure 1. Synthesis stages of Copper oxide nanoparticles : (a, b) reddish-brown precursor solution at different reaction stages; (c) translucent light green precursor solution before reaction; (d) supernatant after centrifugation and purification.

International Journal of Environmental Sciences
ISSN: 2229-7359
Vol. 11 No. 24s, 2025
https://theaspd.com/index.php

3. RESULT AND DISCUSSION

3.1 Point of zero charge of Copper oxide nanoparticles

The pzc of nanoparticles made of Copoer oxide nanoparticles was found to be between 7.5 and 8.0 applying the drift technique (Fig 4.1). A point of zero charge could be assessed and an intersecting point were the two value were equal could be found by Plotting the starting and ending pH levels.For readings of pH below the pic, the final pH being higher than the beginning pH indicated protons absorption on the CuO surface. Conversely, for pH values higher than the pzc, the final pH decreased compared to the initial pH due to OH^- adsorption. This behavior confirms that the Copper oxide nanoparticles possess a slightly basic surface nature [20].

Figure. 2 Effect of point of zero charge of Copper oxide nanoparticles

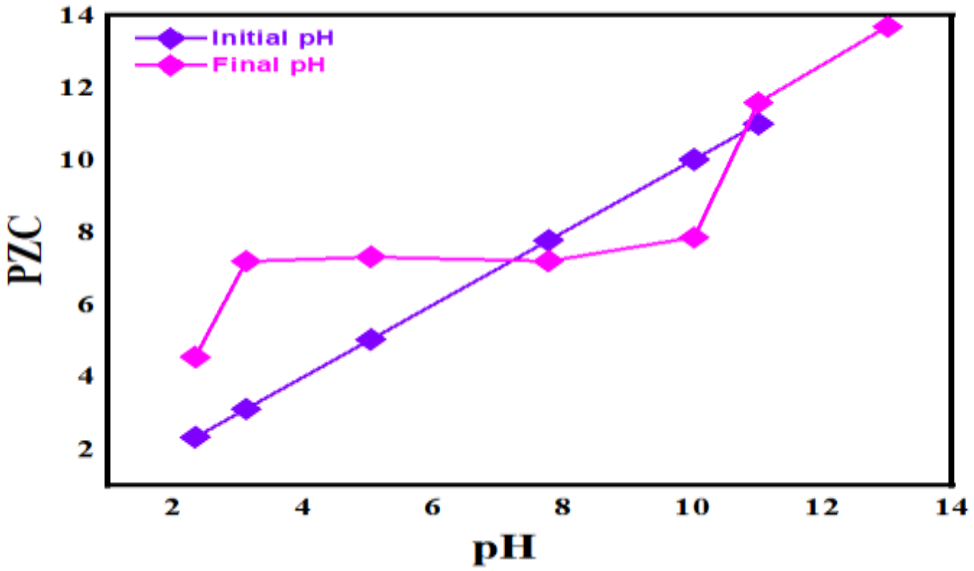

To further support this observation, the variation in pH of Copper oxide nanoparticles at different initial concentrations over 24 and 48 hours is presented in Table 1.

Table 1. Variation in pH over time for different adsorbents, including copper oxide nanoparticle, at different concentration

	Amount (g)	Initial pH	Final pH	
			After 24 hrs.	After 48 hrs.
Adsorbent Copper NANO Particle	0.4	2.34	4.55	4.56
	0.4	3.12	7	7.2
	0.4	5.04	7.15	7.32
	0.4	7.78	7.49	7.21
	0.4	10.02	7.48	7.87
	0.4	11.01	11.87	11.6

3.2 BET Analysis

The nitrogen adsorption–desorption isotherm of synthesized Copper Oxide Nanoparticles exhibited a typical Type IV isotherm with an H_3 hysteresis loop, confirming the mesoporous nature of the material. The isotherm rose gradually at low relative pressures (P/P_0) and sharply at higher P/P_0 values, consistent with capillary condensation in mesopores. The linear BET plot (P/P_0 = 0.05–0.30) showed a strong correlation coefficient (R^2 = 0.9769), indicating the reliability of the model. The slope and intercept of the BET line were 0.0043 and 0.0826, respectively, from which the monolayer adsorbed gas volume (Vm) was calculated as 11.5 cm^3/g. The corresponding BET constant was 30, while the BET surface area was determined to be ~30 m^2/g, slightly higher than values reported for similar nanostructured oxides. The total pore volume was ~0.082 cm^3/g, and the average pore diameter was ~6.8 nm, placing the material in the mesoporous range (2–50 nm). Pore size distribution analysis further confirmed that most pores were concentrated in the 2–10 nm range.

These results highlight that the synthesized Copper Oxide Nanoparticles possess a moderate surface area with well-developed mesoporous channels, providing abundant accessible sites for adsorption. The combination of mesoporosity and enhanced surface area supports efficient diffusion and uptake of cationic pollutants such as

methylene blue, especially under favorable pH conditions (pH > PZC ~7.5–8.0), where electrostatic interactions dominate [22,23].

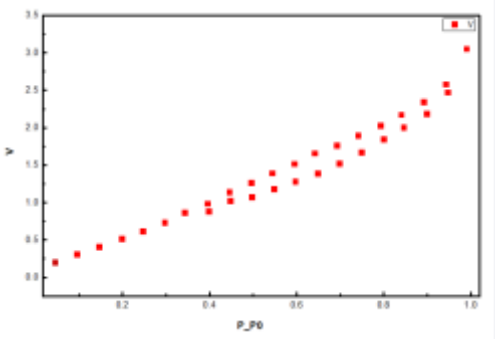

Fig. 3(a)

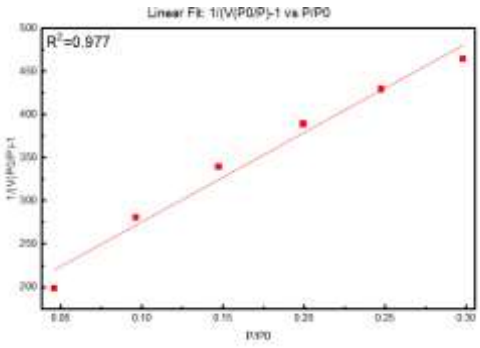

Fig. 3(b)

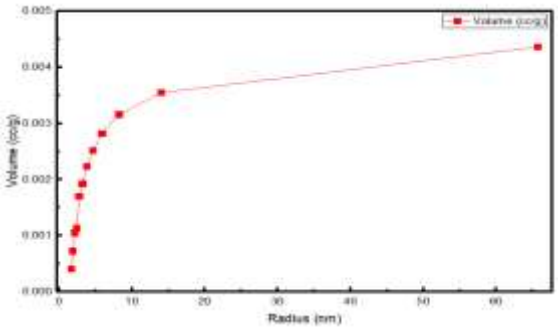

Fig. 3(c)

Figure 3. BET analysis of Copper oxide nanoparticles : (a) N_2 adsorption–desorption isotherm, (b) BET linear plot for surface area determination (R^2 = 0.977), (c) pore size distribution curve.

3.3 Field Emission Scanning Electron Microscope (FESEM) Analysis

This is a sophisticated method that allows for the examination of materials' surface morphology and microstructure in great detail. Copper oxide nanoparticles were produced via the chemical reduction technique and characterized accordingly [24]. FESEM (Their distribution and morphology were examined using field-emitting scanning electron microscopy).

In preparation for the FESEM analysis, a sample of the copper oxide nanoparticles that had been produced was collected. In most cases, this involves distributing the nanoparticles over a conductive substrate, which could be a silicon wafer or a copper grid coated with carbon. To investigate the morphology and microstructure of the copper nanoparticles, FESEM photographs of the sample were taken at a number of different magnifications. It is recommended that the FESEM analysis be performed once more on additional samples in order to guarantee consistency and produce findings that are statistically significant.

FESEM was used to investigate the product's morphology. The images in Fig. 4a–c are scans of nanoparticles obtained using an electron microscope. Through this, the production of flower-like microstructures composed of copper oxide nanoparticles was demonstrated. The structures appear as hierarchical flower-like aggregates, with individual nanosheets or nanorods having thicknesses in the range of 50–200 nm.

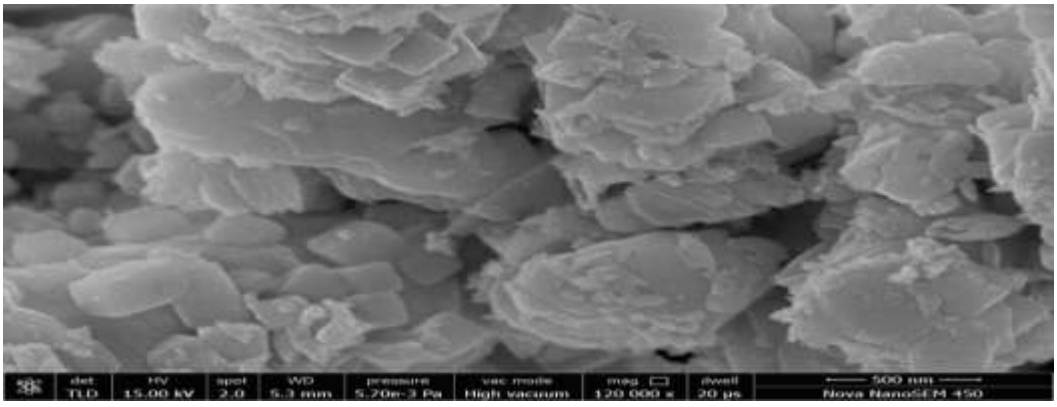

Fig.4 (a)

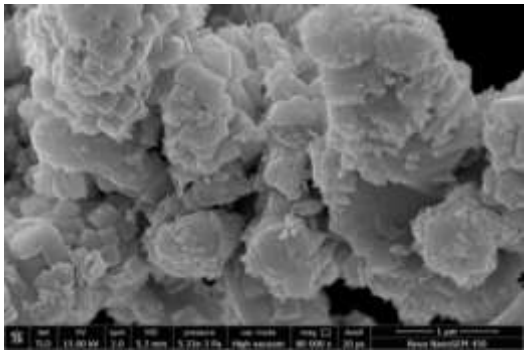

Fig.4 (b)

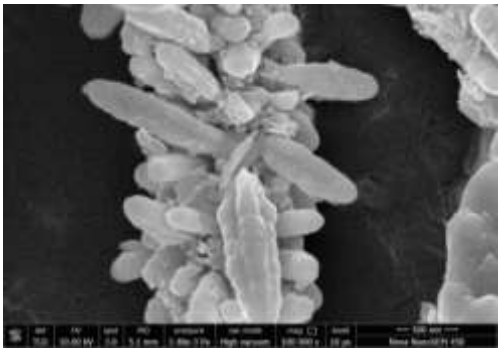

Fig.4 (c)

Figure 4 FESEM images of Copper oxide nanoparticles : (a) Surface morphology at high magnification, (b) after interaction with CV showing an aggregated structure, and (c) after interaction with MB showing porous and layered morphology

3.4 Fourier Transform Infrared (FTIR) Studies

FTIR spectra (400–4000 cm^{-1}) were used to identify functional groups in synthesized and dye-loaded CuO nanoparticles (Fig. 5a–5c). For pure Copper oxide NPs (Fig. 5a), a broad absorption band at 3432 cm^{-1} corresponds to O–H stretching from adsorbed water or surface hydroxyl groups, while peaks at 2923 cm^{-1} indicate C–H stretching from residual organic matter. The band at 2348 cm^{-1} suggests adsorbed CO_2, and peaks at 1688 and 1632 cm^{-1} represent bending vibrations of water molecules. A distinct peak at 1084 cm^{-1} confirms C–O stretching, while the strong band at 521 cm^{-1} is attributed to Cu–O vibrations, validating CuO nanoparticle formation [25].

For CV-loaded CuO (Fig. 5b), spectral shifts indicate interaction between CuO surfaces and CV dye via electrostatic attraction. In MB-loaded CuO (Fig. 5c), new peaks at 1636 cm^{-1} (N–H bending/aromatic C=C stretching), 1420 cm^{-1} (aromatic ring vibrations), and 963 cm^{-1} (C–N stretching) confirm MB adsorption [26]. These results show that hydroxyl and organic functional groups on CuO surfaces play a key role in dye binding, where negatively charged CuO groups interact electrostatically with cationic MB molecules.

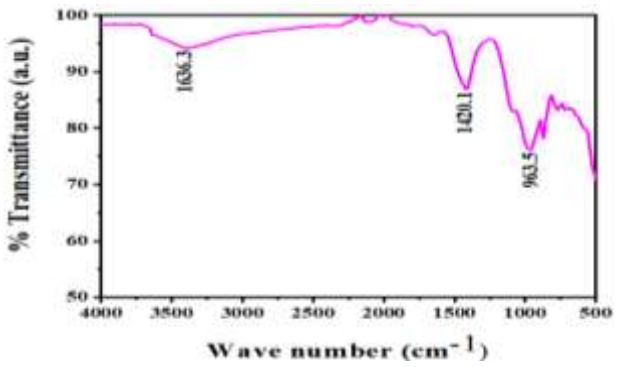

Fig. 5 (a)

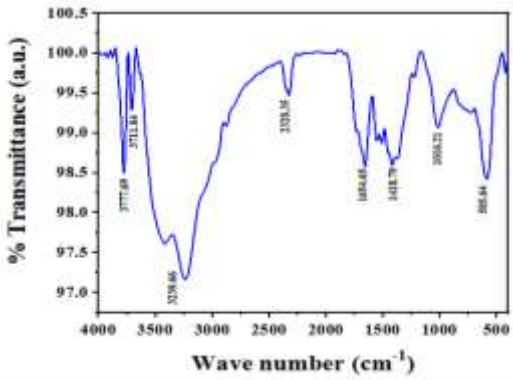

Fig 5 (b)

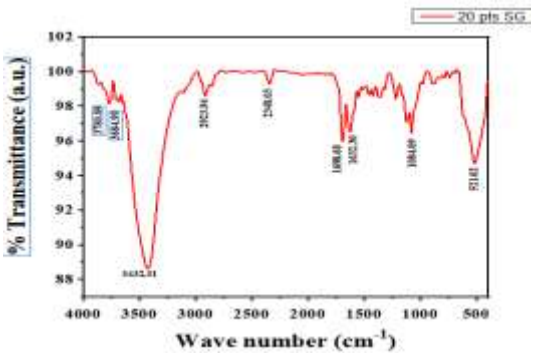

Fig 5 (c)

Figure 5. FTIR spectra: (a) synthesized copper oxide nanoparticles, (b) loaded CV dye, (c) loaded MB dye.

3.5 UV-Visible spectroscopy

Copper oxide nanoparticles were characterized using UV–Visible spectroscopy. The absorption spectrum (Figure 4.9) showed a strong band at 280–300 nm, linked to intrinsic electronic transitions, with maximum absorbance at ~265 nm (0.55). The calculated band gap was 4.7 eV. The absence of a peak near 580 nm confirmed no

metallic copper impurities, and the spectrum matched earlier reports, verifying successful synthesis with good optical stability. After interaction with MB dye, a peak appeared at 650–670 nm (Figure 4.10), with the band gap reduced to ~2.0–2.1 eV, confirming dye adsorption. Similarly, spectra in the 550–600 nm range (Figure 5.7) revealed a surface plasmon resonance band around 580 nm, indicating sensitivity to surface chemistry and particle size. A distinct peak at 600–620 nm (Figure 5.4b) further confirmed CV adsorption, with a calculated band gap of ~2.4 eV.

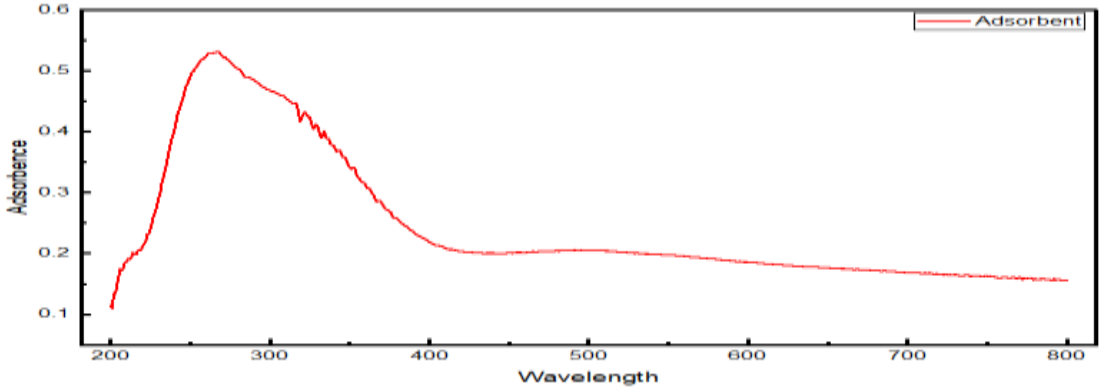

6(a). UV- Vis spectrumof Copper Oxide Nanoparticles

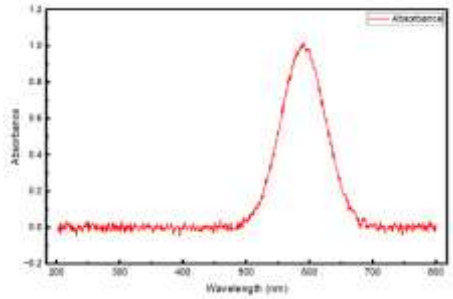

6(b) UV- Vis spectrumof Copper Oxide loaded

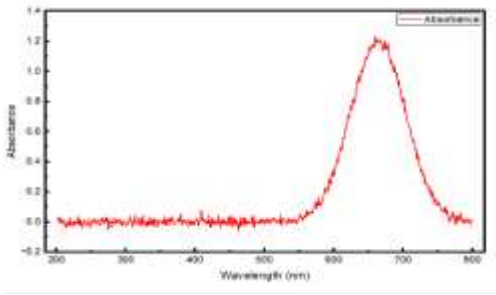

6(c) UV- Vis spectrumof Copper Nanoparticles of CV Oxide Nanoparticles of MB loaded

3.5 Fixed-bed Column Study

3.5.1 Effect of pH

The fluids with pH levels between 2 to 10 on the uptake of methylene blue, or MB, onto Copper oxide nanoparticles was evaluated using 0.50 g of absorption in 50 mL solution at a beginning methylene blue concentration of 50 mg L^{-1}. A calibration curve and ultraviolet-visible spectrophotometry at roughly 664 nm were used to determine the remaining MB concentration following 90 minutes of stirring the solutions at 180 rpm.

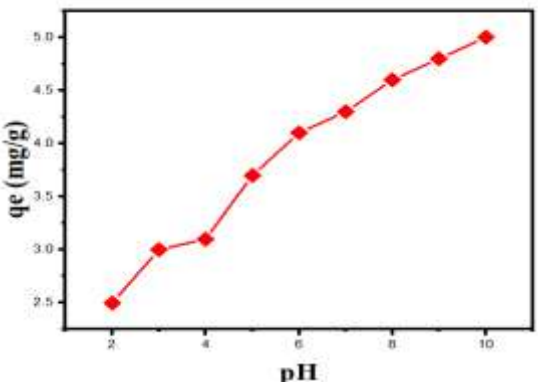

Fig.7 (a)

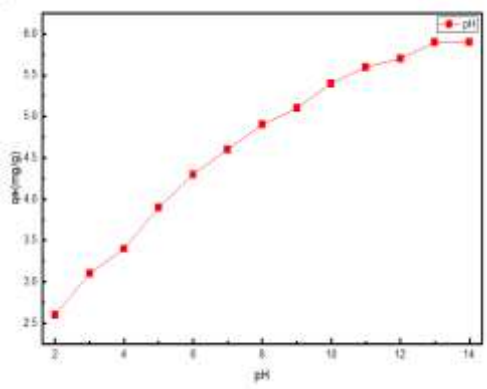

Fig. 7 (b)

Figure 7. Effect of pH on dye adsorption onto copper oxide nanoparticles : (a) adsorption of CV and (b) adsorption of MB

As shown in Fig. 7a, the equilibrium uptake (q_e) increased monotonically from ~2.5 to ~5.0 mg g^{-1} with increasing pH. A similar trend was observed for CV adsorption (Fig. 7b), where q_e also increased steadily with rising pH values.

This behavior is attributed to the surface charge of copper oxide nanoparticles relative to its point of zero charge (pzc ≈ 7.5–8.0). At low pH, protonation of surface sites and competition from H^+ ions suppress adsorption of the cationic dye, whereas at pH > pzc the surface becomes negatively charged, enhancing electrostatic attraction and thus increasing q_e [27]. The equilibrium uptake was calculated using

$$q_e = \frac{(C_0 - C_e)\,V}{m}$$

In this case, V (L) stands for the mass of the adsorbent, m (g), for the volume of the solution, and C_0 and C_e (mg·L^{-1}) for the first and optimum dye concentrations, respectively. Up to pH 10, no decrease was seen within the range under investigation.

3.5.2 Impact of various adsorbent dose

An investigation was conducted using Copper oxide nanoparticles to investigate how the adsorbent amount affects the effectiveness of CV dye removal. The adsorbent dose was varied from 50 mg to 120 mg, while the dye concentration was kept constant. As given in Fig. 8a, As the adsorbent dosage increased, the % removal of CV rose continuously, reaching a maximum of about 96% at 120 mg. This enhancement in removal efficiency can be explained by the increased adsorbent dosages and larger number of accessible empty adsorption sites, which allows more dye molecules to interact with the nanoparticles [28]. However, beyond 100 mg, the increase in removal efficiency became less significant, indicating that the system was approaching equilibrium. At this stage, most dye molecules were already adsorbed, and additional nanoparticles only provided excess unutilized sites. Therefore, while increasing the adsorbent dose improves dye removal efficiency, doses above 100 mg do not contribute proportionally to removal and may be considered less economical.

The impact of several dosages of nanoparticles made of Copper oxide nanoparticles on MB removal was also examined at a predetermined content of 50 mg L^{-1} of methylene blue, pH 2, temperature of 300 K, and rotating speed of 500 rpm. Doses of Copper oxide nanoparticles varied from 50 to 120 mg. As illustrated in Fig. 8b, At 1.503 mg g^{-1} to 4.688 mg g^{-1}, the adsorption capacity rose, and the percentage of MB-eliminated increased from 20.06% at 50 mg to 93.76% at 120 mg [29].

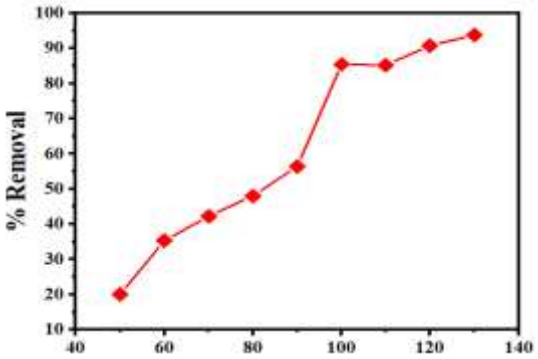

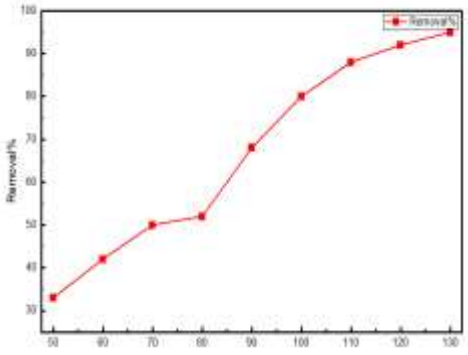

Fig. 8 (a) **Fig. 8(b)**

Figure 8. Effect of adsorbent dose on dye removal using Copper oxide nanoparticles : (a) percentage removal of CV and (b) percentage removal of MB

3.5.3 Effect of Bed Heights

Using Copper oxide nanoparticles in a fixed-bed column, Figures 9a and 9b illustrate how bed depth affects the groundbreaking action of CV and MB adsorption.

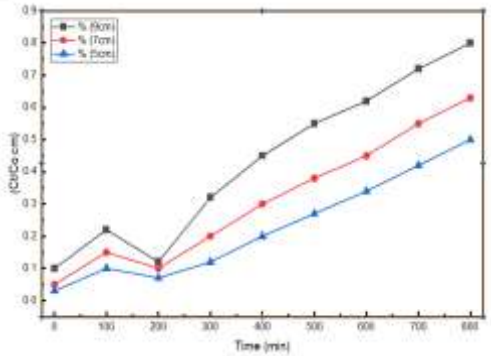

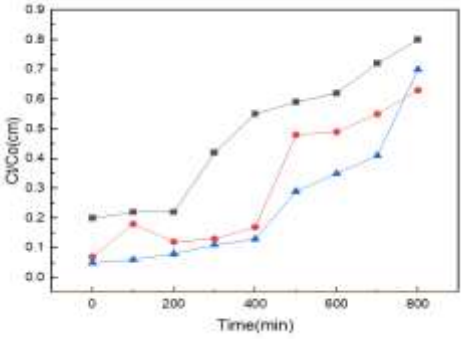

Fig. 9 (a) **Fig. 9 (b)**

Figure 9. Effect of different bed heights on dye adsorption in a fixed-bed column using Copper oxide nanoparticles : (a) breakthrough curves for CV and (b) breakthrough curves for MB

The breakthrough curves show that growing the bed height between 10 cm and 15 cm significantly delayed both breakthrough and exhaustion times. At a lower bed height (10 cm), the effluent concentration (Ct/Co) rose sharply, indicating faster saturation of the adsorbent bed and reduced adsorption efficiency. In contrast, the 15 cm bed height exhibited a more gradual increase in Ct/Co, reflecting an extended breakthrough time and prolonged column service life.

Increased surface area accessible for adsorption and a larger amount of adsorbent substance, which offer greater opportunities for dye uptake and lengthen the time of contact with the adsorbent material and MB molecules, are responsible for this enhancement at deeper bed depths. Additionally, the wider mass transfer zone seen at deeper bed depths enhances the effectiveness of dye removal and results in more efficient use of the adsorbent bed[30].

Therefore, it can be concluded that increasing the bed height enhances adsorption performance by delaying breakthrough, extending exhaustion time, and improving overall column efficiency. However, very high bed depths may also lead to higher pressure drops and increased operational costs, so an optimal bed depth should be selected to balance adsorption efficiency with practical feasibility.

3.5.4 Effect of Flow Rate

The breakout of the curve at 5 mg·L^{-1} (influent concentrations) was compared with those at 6 and 9 mL·min^{-1} in order to assess the impact of flow rate on fixed-bed adsorption efficiency.The estimated total adsorption capabilities, derived from quantitative analysis employing trapezoidal integral of the area above the break curves (mass removed = Q∫0t(C0-Ct) dt ,were 6.28 mg·g^{-1} at 6 mL·min^{-1} and 5.96 mg·g^{-1} at 9 mL·min^{-1} (the adsorbent mass = 0.50 g).

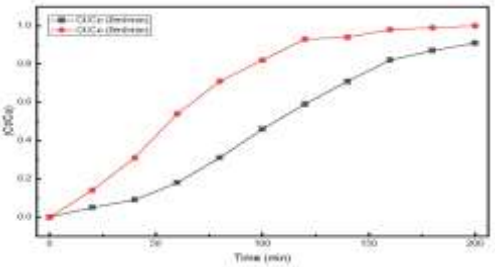

Fig. 10 (a)

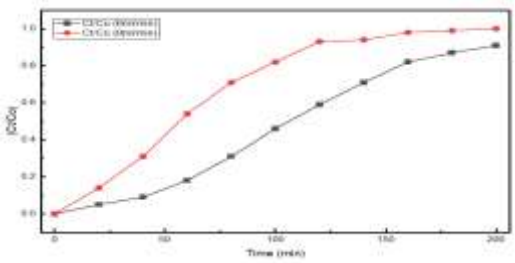

Fig. 10 (b)

Figure 10. Effect of flow rate on breakthrough curves in a fixed-bed column using Copper oxide nanoparticles : (a) CV adsorption at 6 and 9 mL·min^{-1} and (b) MB adsorption at 6 and 9 mL·min^{-1}

As shown in Fig. 10a and b, the higher capacity at the lower flow rate reflects the increased residence time and enhanced mass transfer of dye molecules into the adsorbent pores, which delays breakthrough and promotes fuller utilization of active sites. Conversely, the shorter contact time at 9 mL·min^{-1} leads to earlier breakthrough and slightly reduced bed utilization despite a higher volumetric throughput [31]. The corresponding breakthrough results for CV adsorption at 6 and 9 mL·min^{-1} support the trends observed in Fig. 10a. These results indicate that, for maximum dye removal efficiency in this system, operating at a lower flow rate is preferable, although trade-offs between treatment rate and adsorption efficiency must be considered.

3.5.5 Effect of Temperature and Thermodynamic study

Through an analysis of the thermodynamic properties of biosorption, including ΔG°, ΔH°, and ΔS°, it is possible to establish whether the biosorption process is feasible from a thermodynamic standpoint. In these experiments, the equilibrium constant or K was exchanged with the Langmuir isotherm constant (b), expressed in L·mol^{-1}. For the biosorption of MB, the changes in entropy (ΔS°) and enthalpy (ΔH°) were computed using Fig. 10a and b, which show the ln(b) vs. 1/T plot's slope and intercept [32].

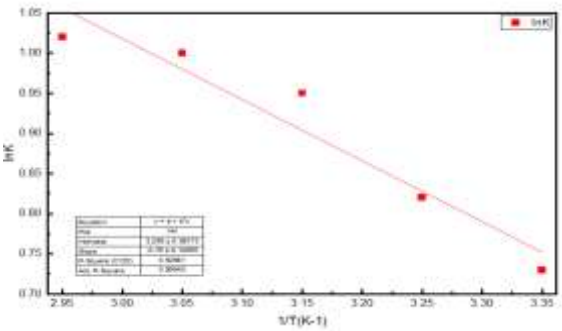

Fig. 11 (a)

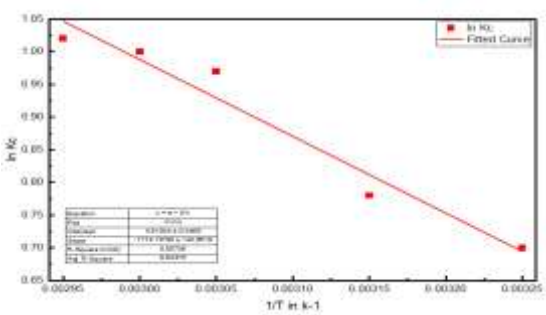

Fig. 11 (b)

Figure 11. Thermodynamic study of dye adsorption onto Copper oxide nanoparticles : (a) Van't Hoff plot (lnK vs. 1/T) for CV and (b) Van't Hoff plot (lnK vs. 1/T) for MB

Since computed ΔG° values were negative, the method of biosorption was confirmed to be spontaneous. Furthermore, a decrease in biosorption was seen as the temperature rose. While the increased ΔS° value of 27.42 J·mol^{-1}·K^{-1} suggests an increase in stability at the interface between the solid and the solvent, the elevated ΔH° value of 6.49 kJ·mol^{-1} implies an endothermic biosorption process. Together, these two thermodynamic elements improve the process's feasibility and spontaneity.

3.5.6 Kinetics

Kinetic of adsorption of MB on synthesized copper oxide nanoparticle was performed using 50 mg of MB concentration. Adsorbent dose used was 500 mg and pH were maintained between 2–3 and prepared nanoparticle uptake of MB was observed at predetermined intervals of time between 10 to 180 min. Considering the slope of log Plotting (qe-qt) against time, displaying the first-order constant of rate k_1 value was determined. Values 0.0035 to 0.0025 (MB) obtained at different concentrations give a hint on possibility that intraparticle diffusion process as part of adsorption process which do not affect the rate-controlling step.

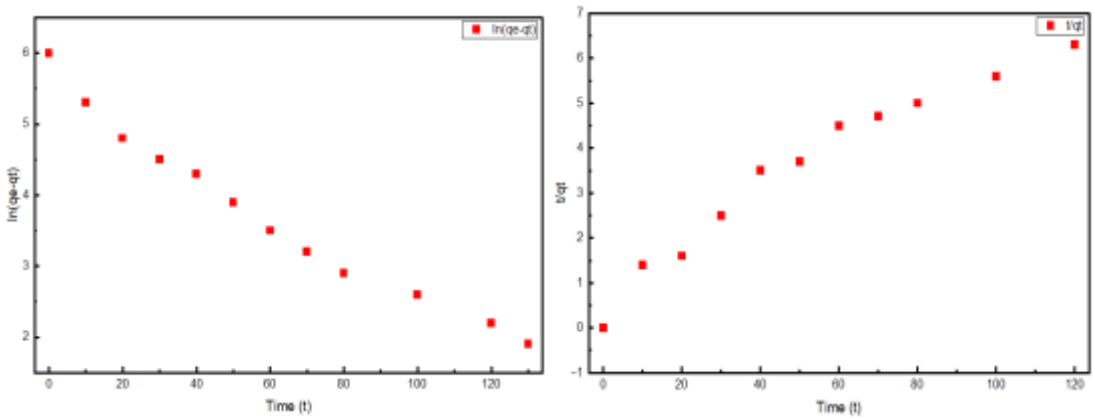

Fig. 12 (a) **Fig. 12** (b)

Figure 12. Kinetic modeling of MB adsorption onto Copper oxide nanoparticles : (a) pseudo-first-order (PFO) model and (b) pseudo-second-order (PSO) model

The adsorption of MB on Copper oxide nanoparticles followed both pseudo-first-order (PFO) and pseudo-second-order (PSO) kinetics (Figures 12a, 12b). PSO provided a better fit, with higher R^2 and qe,cal values close to qe,exp, confirming chemisorption as the dominant mechanism, while PFO indicated minor physisorption. Intraparticle diffusion contributed but was not the sole process. Overall, the PSO model best described the adsorption, suggesting electron sharing between CuO functional groups and dye molecules. The rate constant (k_2) and qe values were determined from the linear plot using slope and intercept. To ascertain the pseudo- first and second reactions of the reaction andthe minimal communication time of the adsorbent, the kinetics of adsorption of crystal violet (CV) dye onto produced copper nanoparticles were studied. The studies used a pH range of 2–3, 500 mg of adsorbent, and a starting CV level of 50 mg·L^{-1}.The adsorption behavior was examined for different contact durations that range from to 180 minutes.

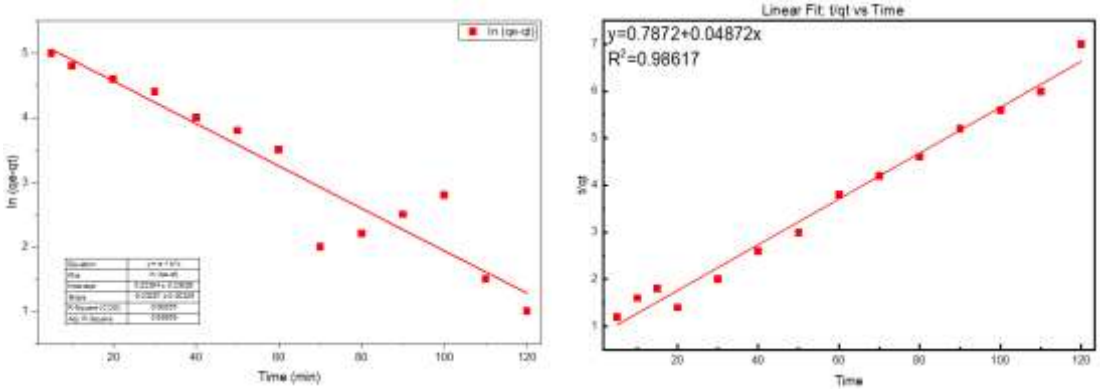

Fig 13 (a) **Fig. 13** (b)

Figure 13. Kinetic modeling of MB adsorption onto Copper oxide nanoparticles: (a) pseudo-first-order (PFO) model and (b) pseudo-second-order (PSO) model

In The rate constant (k_1) was estimated using the pseudo-first-order model and regression charts of $\ln(q_e-q_t)$ versus time or adsorption capacity (q_e) (Fig. 13a). The correlation coefficients (R_2) varied between 0.882 and 0.996,

while the qe values from 15.33 to 97.32 mg·g^{-1}. The estimated and actual qe values continued to differ, suggesting the the model's consistency with the data from experiments was only moderate. This suggests that the model of pseudo-first order could not adequately explain the absorption of CV on particles of copper. The outcomes of the trial were more closely correlated with the model of pseudo-second order (Fig. 13b).In the t/qt vs. t graphs, the straight lines indicated higher R_2 values (0.784–0.996). The calculated qe value closely corresponded to the experimental results, and the higher R_2 values indicate that the pseudo-second-order model best describes adsorption. According The most widely used method for this concept is chemisorption, which entails the transfer of electrons between the functional regions of the dye molecules with copper nanoparticles [33].Overall, chemisorption plays a significant role as the pseudo-second-order model in the process more precisely depicts the rate at which CV absorbs onto nanoparticles of copper than the pseudo-first-order model.

3.5.7 BDST model

The effect of bed height on MB and CV adsorption by CuO nanoparticles was studied using the Bed Depth Service Time (BDST) model. Breakthrough curves were evaluated at Cb/Co ratios of 0.05, 0.08, and 0.10 for bed heights of 10, 12, and 15 cm (Fig. 13a–b, Fig. 5.24). In all cases, a linear relationship between service time and bed depth confirmed that the BDST model accurately describes column dynamics. Service time increased proportionally with bed height due to greater adsorption site availability and longer adsorbate–adsorbent interaction. At Cb/Co = 0.05, service time rose from ~52 min (10 cm) to ~108 min (15 cm); at 0.08, from ~45 min to ~95 min; and at 0.10, from ~38 min to ~82 min. These results show that stricter breakthrough limits shorten column lifespan. The high correlation coefficients ($R^2 > 0.97$) from linear fitting validate the model's reliability. Overall, CuO nanoparticles proved effective for MB and CV removal in fixed-bed systems, and the BDST model demonstrates strong potential for scaling adsorption processes to industrial applications.

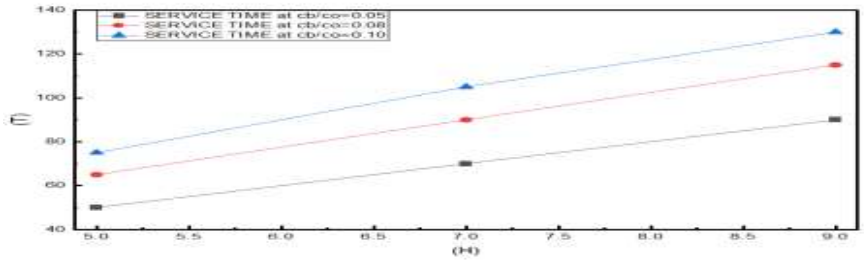

Figure 13.(a) Bed Depth Service Time (BDST) model for MB adsorption nto Copper oxide nanoparticles

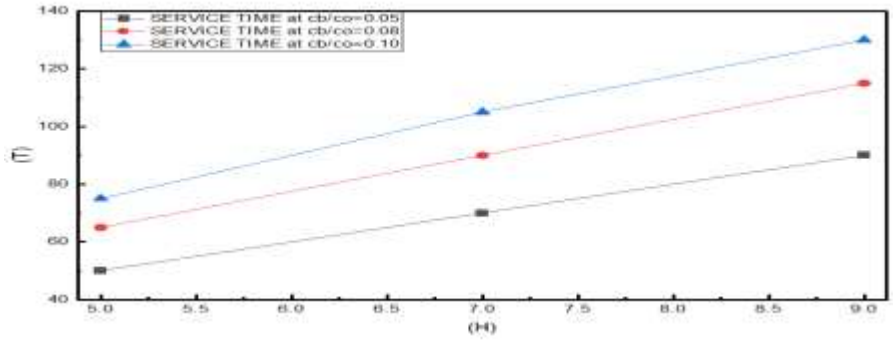

Figure 13.(b) Bed Depth Service Time (BDST) model for CVadsorption onto Copper oxide nanoparticles

3.5.8 Thomas model

The Thomas model was used to assess how well methylene blue adsorbed onto Copper oxide nanoparticles in a column with a fixed bed. As shown in Fig. 14(a) (b), the linearized Thomas plots of $\ln[(C_0/Ct) - 1]$ versus service time (t) produced straight lines with high correlation coefficients (R^2 values close to unity), proving the Thomas model's applicability in explaining the column adsorption process [35] .The negative slopes correspond to the adsorption rate constant (kTh), in contrast, the intercepts are associated with the bed's maximal adsorption capacity (q_0). *The Thomas model effectively described MB and CV adsorption onto CuO nanoparticles in fixed-bed columns. Variations in operating conditions significantly influenced model parameters. Increased bed height enhanced adsorption capacity (q_0) by providing more active sites and longer contact time, while higher influent concentrations boosted mass transfer, further raising q_0. Conversely, higher flow rates reduced q_0 due to insufficient contact time. Model fits showed strong linearity (R^2 = 0.803–0.986), and parameters (kTh, q_0) were derived from slope and intercept values. Overall, the Thomas model reliably predicted breakthrough behavior and adsorption performance, supporting its application in large-scale fixed-bed systems.*

International Journal of Environmental Sciences
ISSN: 2229-7359
Vol. 11 No. 24s, 2025
https://theaspd.com/index.php

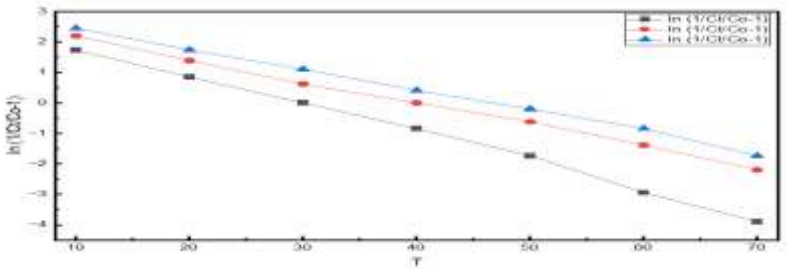

Figure 14. (a)Thomas Model of MB

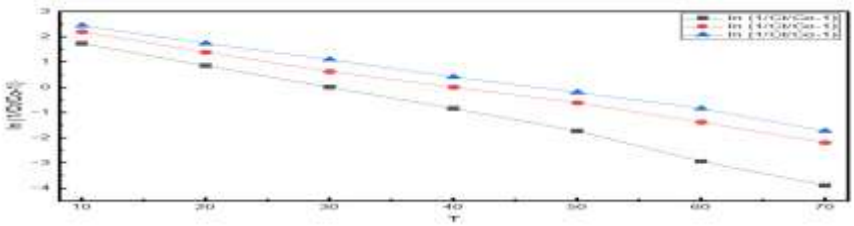

Figure 14.(b) Thomas Model of CV

3.5.9 Yoon Nelson Model for CV and MB Adsorption onto Copper Oxide Nanoparticles

The Yoon–Nelson model was applied to evaluate the breakthrough behavior of crystal CV adsorption onto Copper Oxide Nanoparticles in the fixed-bed column, and the corresponding plots of ln Figure 15(a) (b), the linear relationships obtained under different operating conditions produced high coefficients of determination ($R^2 > 0.95$), confirming that the Yoon–Nelson model reliably describes the experimental data. From the slope and intercept values, the rate constant (k_{YN}) and the 50% breakthrough time (τ) were calculated. The results indicated that τ increased consistently with increasing bed height, rising from ~48 min at 5 cm to ~95 min at 15 cm, reflecting extended contact time and larger adsorbent mass. Similarly, at higher influent concentrations (3–10 mg/L), τ values decreased due to faster saturation of active sites, while k_{YN} values increased, showing a stronger driving force for mass transfer at higher loading. In contrast, increasing the flow rate from 6 to 9 mL/min reduced τ (from ~88 min to ~63 min), as shorter residence times limited adsorption efficiency. These findings demonstrate that the Yoon–Nelson model successfully predicts breakthrough profiles and provides simple yet reliable parameters for assessing and scaling up CV removal by Copper Oxide Nanoparticles in fixed-bed adsorption systems

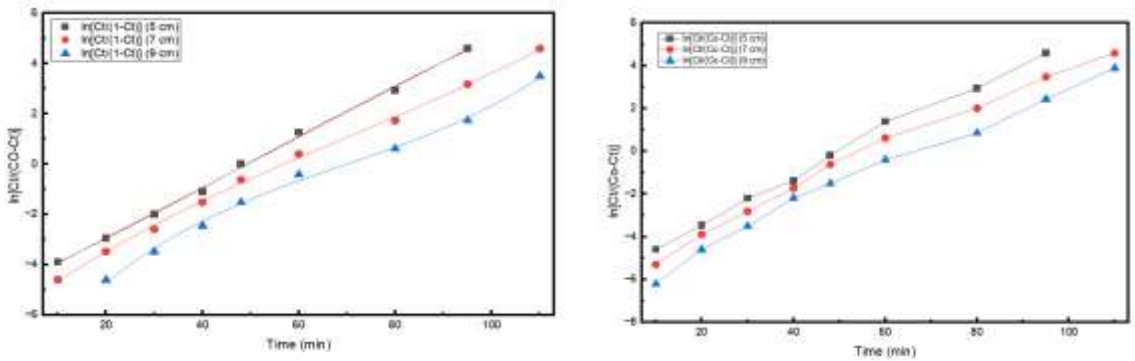

Figure15.(a), 15 (b): Yoon Nelson Model of CV and MBAdsorption

3.5.10Admas- Bohart Model for CV and MB Adsorption onto Copper Oxide Nanoparticles

The Adana's- Bohart model was employed to analyse the initial portion of the breakthrough curves for CV adsorption onto Copper oxide nanoparticles in the fixed bed coloum, and the corresponding plots are shown in Figure 16(a), (b). The liener trendobtained confirmed that the model adequately describes the early breakthrough regions , with correlation coefficients (R^2) ranging between 0.86 and 0.94 depending on the operating conditions. From the slope and intercept values, the kinetic constant (k_{AB}) and the maximum adsorption capacity (N_0) of the bed were determined. The results revealed that increasing bed height from 10 to 15 cm led to higher N_0 values (from ~120 to ~168 mg/L), reflecting the larger quantity of adsorbent available for uptake, while kAB decreased slightly, indicating slower breakthrough due to extended diffusion paths. In contrast, raising the influent dye concentration from 3 to 10 mg/L resulted in higher kAB values and reduced bed service time, as greater concentration gradients accelerated mass transfer and saturated the sites more quickly. Similarly, increasing flow rate from 6 to 9 mL/min increased k_{AB} but decreased N_0, since faster flow reduced the effective contact

time between adsorbent and adsorbate. These findings confirm that the Adams–Bohart model is particularly useful for predicting the early stages of column operation and provides valuable insight into the influence of bed depth, concentration, and flow rate on the adsorption dynamics of CV onto Copper Oxide Nanoparticles.

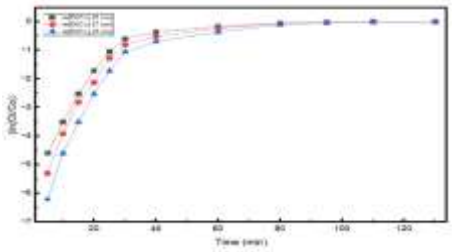

Figure 16(a): Admas Bohart of MB

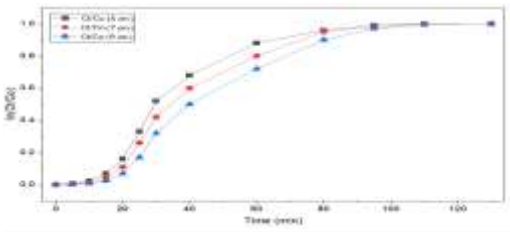

Figure 16(b): Admas Bohart Model ofCV

Comparison of Fixed Bed Model Results ~ MB on Copper Oxide Nanoparticles

Model	Parameters	Value	R^2	X^2	SSE
Bohart- Admas	$L.min^{-1}.mg^{-1}$	0.0039	0.906	1.003	0.221
Thomas	$L.min^{-1}.mg^{-1}$	0.0039	0.991	1.004	0.223
Yoon- Nelson	min^{-1}	0.0796	0.906	1.003	0.22
BDST	$L.min^{-1}.mg^{-1}$	0.00123	0.912	0.998	0.210

Comparison of Fixed Bed Model Results ~ CV on Copper Oxide Nanoparticles

Model	Parameters	Value	R^2	X^2	SSE
Bohart- Admas	$L.min^{-1}.mg^{-1}$	0.0031	0.0952	1.021	0.267
Thomas	$L.min^{-1}.mg^{-1}$	0.0054	0.991	1.004	0.182
Yoon- Nelson	min^{-1}	0.027	0.975	1.008	0.201
BDST	$L.min^{-1}.mg^{-1}$	0.013	0.980	1.010	0.225

4. CONCLUSION

In order to effectively remove the pigments Crystal Violet and Methylene Blue form aqueous solutions, the current study shows how to produce and use nanoparticles of copper oxide in a fixed- bed column. Through careful characterisation, their appropriateness as adsorbents was confirmed: A mesoporous structure with an exterior area of about 20–27 $m^2 \cdot g^{-1}$ was revealed by BET analysis. FESEM images showed nanoscale flower-like and quasi-spherical shapes; and FTIR spectrum analysis showed Cu–O vibrations that stretched and stabilizing functional groups.Approximately 7.5 to 8.0 was found to be the point of zero charge, confirming that adsorption efficiency is strongly influenced by solution pH. Batch and column studies further demonstrated the adsorption potential of copper oxide nanoparticles under varying operational conditions. Adsorption capacity increased at pH values above the pHpzc, as negatively charged CuO surfaces enhanced electrostatic attraction with cationic dyes. Increasing the adsorbent dose from 50 mg to 120 mg significantly improved removal efficiency, achieving up to ~96% for CV and ~93% for MB. Higher bed heights delayed breakthrough and exhaustion times, extending column service life, whereas higher flow rates reduced contact time and slightly decreased adsorption capacity. Thermodynamic analysis revealed that the adsorption process was endothermic (positive $\Delta H° = 6.49$ $kJ \cdot mol^{-1}$) and spontaneous (negative $\Delta G°$), accompanied by increasing unpredictability (positive $\Delta S° = 27.42$ $J \cdot mol^{-1} \cdot K^{-1}$). In both MB and CV kinetics studies, adsorption was shown to follow a pseudo-second-order model by higher R_2 values and a better agreement between qe,cal and qe,exp when compared to the pseudo-first-order model. This suggests that chemisorption is the main mechanism, with intraparticle diffusion acting as a fallback.. Overall, Copper oxide nanoparticles proved to be highly efficient adsorbents for cationic dyes in fixed-bed systems, combining favorable physicochemical characteristics with excellent adsorption capacity. Their effectiveness under optimized conditions (pH 7–9, bed height 6–9 cm, and moderate flow rate) underscores their promise for wastewater treatment applications. Future investigations should focus on column regeneration and large-scale implementation to establish Copper oxide nanoparticles as cost-effective and sustainable adsorbents for industrial effluent treatment.

REFERENCES

[1]. Sinha, T., & Ahmaruzzaman, M. (2015). Green synthesis of copper nanoparticles for the efficient removal (degradation) of dye from aqueous phase. *Environmental Science and Pollution Research, 22*(24), 20092–20100.

[2]. Das, H. S., Mishra, S., & Roymahapatra, G. (2024). Graphene oxide in water treatment from adsorption to photocatalysis. In *Carbon-Based Materials and Environmental Remediation: Graphene, Biochar, and More* (pp. 137–168). IGI Global.
[3]. Das, R., Roymahapatra, G., & Sinha, I. (2020). Adsorption characteristics of Indian neem leaves (Azadirachta indica) for removal of methyl violet dye from its aqueous solution: Isotherms & kinetics. *Journal of Critical Reviews, 7*, 4196–4209.
[4]. Ghosh, K., Bar, N., Roymahapatra, G., Biswas, A. B., & Das, S. K. (2022). Adsorptive removal of toxic malachite green from its aqueous solution by Bambusa vulgaris leaves and its acid-treated form: DFT, MPR and GA modeling. *Journal of Molecular Liquids, 363*, 119841.
[5]. Rafique, M. A., et al. (2022). Effective removal of Direct Orange 26 dye using copper nanoparticles synthesized from Tilapia fish scales. *Desalination and Water Treatment, 272*, 259–265.
[6]. Rafique, M. A., et al. (2022). Green synthesis of copper nanoparticles using Allium cepa (onion) peels for removal of Disperse Yellow 3 dye. *Desalination and Water Treatment, 272*, 259–265.
[7]. Sinha, T., & Ahmaruzzaman, M. (2015). High-value utilization of egg shell to synthesize silver and gold-silver core shell nanoparticles and their application for the degradation of hazardous dyes from aqueous phase—A green approach. *Journal of Colloid and Interface Science, 453*, 115–131.
[8]. Amoneit, D., Weckowska, S., Spahr, S., Wagner, O., Adeli, M., Mai, I., & Haag, R. (2024). Green chemistry and responsible research and innovation: Moving beyond the 12 principles. *Journal of Cleaner Production, 484*, 144011.
[9]. Roymahapatra, G., Hait, M., Akitsu, T., & Sinha, C. (2025). Chemistry and sustainability: A paradigm shift in chemistry research. *ES Chemistry and Sustainability*.
[10]. Gooijer, F. (2022). The role of chemistry in improving the environment around us. *Global Journal of Environmental Science and Technology, 10*(1), 1–2.
[11]. Mali, S. C., Dhaka, A., Githala, C. K., & Trivedi, R. (2020). Green synthesis of copper nanoparticles using Celastrus paniculatus Willd. leaf extract and their photocatalytic and antifungal properties. *Biotechnology Reports, 27*, e00518.
[12]. Khan, S., Noor, T., Iqbal, N., & Yaqoob, L. (2024). Photocatalytic dye degradation from textile wastewater: A review. *ACS Omega, 9*(20), 21751–21767.
[13]. Tomar, R., Abdala, A. A., Chaudhary, R. G., & Singh, N. B. (2020). Photocatalytic degradation of dyes by nanomaterials. *Materials Today: Proceedings, 29*(4), 967–973.
[14]. Roy, N. T., Paira, P., & Chakrabarty, R. (2025). Selenium-based nanomaterials: Green and conventional synthesis methods, applications, and advances in dye degradation. *RSC Advances, 15*, 3008–3025.
[15]. Lee, S. Y., Kang, D., Jeong, S., Do, H. T., & Kim, J. H. (2020). Photocatalytic degradation of rhodamine B dye by TiO_2 and gold nanoparticles supported on a floating porous polydimethylsiloxane sponge under ultraviolet and visible light irradiation. *ACS Omega, 5*(8), 4233–4241.
[16]. Bhat, M., Abhilash, M. R., Mamatha, S. V., Das, S., & Roymahapatra, G. (2023). Photocatalytic degradation of dyes by titania/ferric oxide/polyvinyl alcohol nanocomposites. *ES General*.
[17]. Khan, A., Roy, A., Bhasin, S., Emran, T. B., Khusro, A., Eftekhari, A., Moradi, O., Rokni, H., & Karimi, F. (2022). Nanomaterials: An alternative source for biodegradation of toxic dyes. *Food and Chemical Toxicology, 164*, 112996.
[18]. Devika, R., & Chauhan, S. (2020). Biosynthesis of copper nanoparticles using Nerium oleander. *Journal of Nanomaterials & Molecular Nanotechnology, 9*(3).
[19]. Khanna, P. K., Gaikwad, S., Adhyapak, P. V., Singh, N., & Marimuthu, R. (2007). Synthesis and characterization of copper nanoparticles. *Materials Letters, 61*(25), 4711–4714.
[20]. Zhang, W., Yao, Y., Li, K., Huang, Y., & Chen, Y. (2011). Influence of dissolved oxygen on aggregation kinetics of citrate-coated silver nanoparticles. *Environmental Pollution, 159*(12), 3757–3762.
[21]. Mishra, A. K., Nayak, A. K., Das, A. K., & Pradhan, D. (2018). Microwave-assisted solvothermal synthesis of cupric oxide nanostructures for high-performance supercapacitor. *The Journal of Physical Chemistry C, 122*(21), 11249–11261.
[22]. Svobodová, E., Tišler, Z., Peroutková, K., Strejcová, K., Abrham, J., Šimek, J., Gholami, Z., & Vakili, M. (2024). Adsorption of Cu(II) and Ni(II) from aqueous solutions using synthesized alkali-activated foamed zeolite adsorbent: Isotherm, kinetic, and regeneration study. *Molecules, 29*(10), 2357.
[23]. Yan, X. C., Chen, K. X., Zhang, G. Y., Peng, M. X., Ma, J. Y., Zang, H. B., & Zhang, F. M. (2024). Nickel single-atom synergistic iron-nitrogen sites for efficient CO_2 electroreduction at a wide potential range. *Chemical Engineering Journal, 498*, 155288.
[24]. Al-Yunus, A., Al-Arjan, W., Traboulsi, H., Schuarca, R., Chando, P., Hosein, I. D., & Hessien, M. (2024). Effect of synthesis conditions on CuO-NiO nanocomposites synthesized via saponin-green/microwave assisted-hydrothermal method. *Nanomaterials, 14*(3), 308.
[25]. Rajamohan, R., Raorane, C. J., Kim, S. C., Ashokkumar, S., & Lee, Y. R. (2023). Novel microwave synthesis of copper oxide nanoparticles and appraisal of the antibacterial application. *Micromachines, 14*(2), 456.
[26]. Priya, M., Venkatesan, R., Deepa, S., Sana, S. S., Arumugam, S., Karami, A. M., & Kim, S. C. (2023). Green synthesis, characterization, antibacterial, and antifungal activity of copper oxide nanoparticles derived from Morinda citrifolia leaf extract. *Scientific Reports, 13*(1), 18838.
[27]. Singh, R., Singh, T. S., Odiyo, J. O., Smith, J. A., & Edokpayi, J. N. (2020). Evaluation of methylene blue sorption onto low-cost biosorbents: Equilibrium, kinetics, and thermodynamics. *Journal of Chemistry, 2020*(1), 8318049.
[28]. Shu, J., Cheng, S., Xia, H., Zhang, L., Peng, J., Li, C., & Zhang, S. (2017). Copper loaded on activated carbon as an efficient adsorbent for removal of methylene blue. *RSC Advances, 7*(24), 14395–14405.
[29]. Yadav, S., Sharma, G., Malik, S., Khyalia, P., & Gupta, A. (2024). Lemon peel-extracted recyclable copper oxide nanoparticles for methylene blue dye adsorption: Optimization, isotherms, kinetics, thermodynamics, and reusability study. *ChemistrySelect, 9*(43), e202404178.
[30]. Asl, M. N., Mahmodi, N. M., Teymouri, P., Shahmoradi, B., Rezaee, R., & Maleki, A. (2016). Adsorption of organic dyes using copper oxide nanoparticles: Isotherm and kinetic studies. *Desalination and Water Treatment, 57*(52), 25278–25287.
[31]. Ibrahim, M. A., & Ibrahim, M. B. (2018). Adsorption of alkali blue, metanil yellow and neutral red dyes using copper (II) oxide particles: Kinetic and thermodynamic studies. *ChemSearch Journal, 9*(2), 13–23.

[32]. Thakur, P., & Kumar, V. (2019). Kinetics and thermodynamic studies for removal of methylene blue dye by biosynthesized copper oxide nanoparticles and its antibacterial activity. *Journal of Environmental Health Science and Engineering, 17*(1), 367–376.
[33]. Srivastava, V., & Choubey, A. K. (2021). Investigation of adsorption of organic dyes present in wastewater using chitosan beads immobilized with biofabricated CuO nanoparticles. *Journal of Molecular Structure, 1242*, 130749.
[34]. Li, T., Fan, J., & Sun, T. (2021). Effective removal of methylene blue dye from water with nanocomposite ceramsites in a fixed-bed column. *Environmental Technology, 42*(24), 3807–3819.
[35]. Ghribi, A., & Chlendi, M. (2011). Modeling of fixed bed adsorption: Application to the adsorption of an organic dye. *Asian Journal of Textile, 1*(4), 161–171.